J. Fluid Mech. (2023), *vol*. 958, A15, doi:10.1017/jfm.2023.75

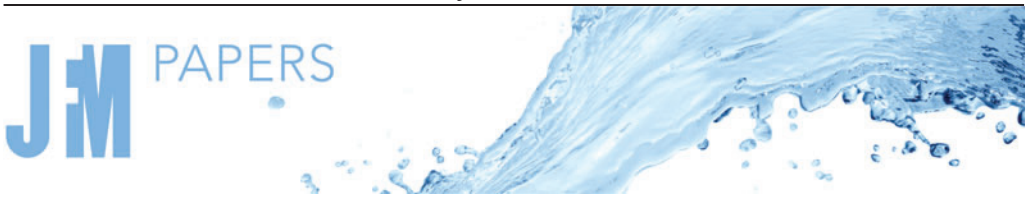

Maximum drag enhancement asymptote in spanwise-rotating viscoelastic plane Couette flow of dilute polymeric solutions

Yabiao Zhu[1,2], Zhenhua Wan[1], Fenghui Lin[1], Nansheng Liu[1,†], Xiyun Lu[1] and Bamin Khomami[3,†]

[1]Department of Modern Mechanics, University of Science and Technology of China, Hefei, Anhui 230026, PR China

[2]Yangzhou Collaborative Innovation Research Institute, Shenyang ADRI, Yangzhou, Jiangsu 225000, PR China

[3]Department of Chemical and Biomolecular Engineering, University of Tennessee, Knoxville, TN 37996, USA

(Received 21 June 2022; revised 16 January 2023; accepted 16 January 2023)

The existence of a maximum drag enhancement (MDE) asymptote at high rotation (*Ro*) and Weissenberg (*Wi*) numbers in turbulent viscoelastic spanwise-rotating plane Couette flow has been demonstrated. Specifically, it is shown that above a critical *Wi*, drag enhancement plateaus and the MDE asymptote is realized in a broad range of *Ro*. The mean velocity profiles at MDE appear to closely follow a log-law profile that has a nearly identical slope but different intercepts as a function of *Ro*. Much like the maximum drag reduction (MDR) asymptote, the logarithmic function in MDE is closely followed if the mean velocity is plotted using the traditional inner variable scaling; however, the logarithmic function is not well defined when examined by the indicator function. Hence, in this study, we have used the logarithmic fit as a visual guide for the mean velocity profile. Last and perhaps the most intriguing finding of this study is that MDE occurs in the elasto-inertial turbulence (EIT) flow state; hence, it is mainly sustained by elastic forces much like the MDR flow state. To that end, a universal picture of elastically induced drag modification asymptotes is emerging, namely these asymptotic states are an inherent property of the elastically sustained EIT flow state.

Key words: viscoelasticity, rotating turbulence

† Email addresses for correspondence: lns@ustc.edu.cn, bkhomami@utk.edu

1. Introduction

It is well known that introducing a trace amount of high-molecular-weight polymers to Newtonian turbulent flows (NT) results in dramatic drag reduction (DR) (Toms 1949; Procaccia, L'vov & Benzi 2008; White & Mungal 2008). Irrespective of the polymer type and polymer–solvent combination, the efficacy of DR increases as the ratio of elastic to inertial forces is increased and eventually saturates at the maximum drag reduction (MDR) asymptote. Moreover, as DR is enhanced, the mean velocity profile changes from the von Kármán log law for NT to the well-known Virk law for MDR (Virk 1975; White, Dubief & Klewicki 2012; Elbing *et al.* 2013). The physical origin of polymer-induced DR has been ascribed to the interaction between polymer chains and turbulent vortices caused by the enhancement of the elongational viscosity observed in dilute polymer solutions as a result of the polymer extension, first postulated by Lumley (1969) and Seyer & Metzner (1969) and then first confirmed through direct numerical simulation calculations of viscoelastic channel flow by Sureshkumar, Beris & Handler (1997). Specifically, the mean shear flow stretches polymers that in turn suppresses small-scale quasi-streamwise vortices (Sureshkumar *et al.* 1997; De Angelis, Casciola & Piva 2002; Dubief *et al.* 2005; Li, Sureshkumar & Khomami 2006, 2015).

Until a decade ago, mechanistic understanding of MDR was one of the most debated topics in turbulent viscoelastic unidirectional parallel shear flows. However, recent definitive experiments and simulations (Choueiri, Lopez & Hof 2018; Lopez, Choueiri & Hof 2019; Shekar *et al.* 2019) have shown that at relatively low Reynolds number, for example $Re \sim 3150$ in pipe flow, as elastic forces are enhanced a reverse transition from NT or elastically modified NT to a laminar flow occurs. In turn, this laminar flow undergoes a secondary instability as elastic forces are further enhanced leading to a new chaotic flow state dubbed 'elasto-inertial turbulence' (EIT) that exhibits DR that is equivalent to MDR. Thus the MDR state is dynamically disconnected from NT. The dominant flow structure in the EIT flow state is that of spanwise-oriented two-dimensional structures that are sustained by both elastic and inertial effects (Samanta *et al.* 2013; Sid, Terrapon & Dubief 2018). At higher Re the laminar flow regime is bypassed and flow directly transitions from an elastically modified NT to the EIT flow state further underscoring the fact that MDR is an EIT flow state irrespective of Re (Choueiri *et al.* 2018).

In sharp contrast to the reverse transition that occurs in DR parallel shear flows, polymer-induced flow relaminarization accompanied by significant drag enhancement (DE) has recently been observed (Zhu *et al.* 2020) in an anticyclonic spanwise-rotating (positive rotation number Ro as defined below) viscoelastic plane Couette flow (RPCF; the zero-curvature limit of Taylor–Couette flow) at relatively low Ro. Despite the opposite drag modification (DM), this relaminarization phenomenon substantiates the universal interplay between turbulent vortices and polymer chains in viscoelastic flow, namely polymer chains stretch in the near-wall region and, in turn, weaken turbulent vortices via extraction of kinetic energy from turbulent motions. At high Ro elastic effects are amplified even at relatively low elasticity number (ratio of elastic to inertial forces) and thus lead to a Coriolis- and elastic-force-driven flow transition from a DR inertial to a DE elasto-inertial turbulent flow (Zhu *et al.* 2022). The dominant coherent structure in the EIT flow state is that of small-scale streamwise-elongated vortices attached to the walls. These vortices cause strong incoherent transport and significant homogenization of polymer stress. Hence, DE in viscoelastic RPCF (Zhu *et al.* 2022) is mainly realized by the interaction of these vortices with polymer chains. To that end, it is rational to expect that a significant increase in elastic forces could lead to a maximum DE (MDE) asymptote in this class of EIT flows.

In this paper, we demonstrate for the first time the existence of a MDE asymptote in the EIT flow state of viscoelastic RPCF. Specifically, it is clearly shown that in a viscoelastic RPCF at high Ro, raising the fluid elasticity, quantified via the Weissenberg number, Wi, results in continuous DE that eventually plateaus as the MDE asymptote is realized. The mean velocity profiles in this novel asymptotic flow state appear to closely follow a log-law profile that has a nearly identical slope but different intercepts as Ro is changed. At MDE the dominant coherent flow structure is that of small-scale streamwise-elongated wall vortices that are almost identical to the EIT flow state in viscoelastic RPCF. Hence much like MDR, this flow state is also mainly sustained by elastic forces.

2. Problem formulation and computational details

The existence of the MDE asymptote in viscoelastic RPCF is explored by direct numerical simulations using a highly efficient three-dimensional spectral parallel algorithm (Liu & Khomami 2013; Teng *et al.* 2018; Song *et al.* 2019; Zhu *et al.* 2020, 2022). We have chosen h, h/U_w, U_w and $\rho {U_w}^2$ as scales for length, time, velocity $\boldsymbol{u}$ and pressure P, respectively. Here, P is the effective pressure, i.e. it includes the contribution of centrifugal force (Salewski & Eckhardt 2015; Brauckmann, Salewski & Eckhardt 2016; Gai *et al.* 2016). The half-gap width is denoted by h, U_w is the wall linear velocity, Ω_z is the spanwise rotation rate and ρ represents the polymeric solution density (see figure 1). The evolution of the polymer conformation tensor $\boldsymbol{C}$ is given by the FENE-P (finitely extensible nonlinear elastic-Peterlin) constitutive equation. This model can quantitatively describe the nonlinear steady shear rheology of nearly constant viscosity dilute polymeric solutions as well as qualitatively capturing their extensional viscosity, in the absence of chain scission. The non-dimensionalized governing equations for an incompressible flow of FENE-P fluids are obtained in a rotating frame of reference with the spanwise rotation rate Ω_z, given as follows:

$$\frac{\partial \boldsymbol{u}}{\partial t} + \boldsymbol{u}\cdot\nabla\boldsymbol{u} = -\nabla P + \frac{\beta}{Re}\nabla^2\boldsymbol{u} + \frac{1-\beta}{Re}\nabla\cdot\boldsymbol{\tau}^p - Ro\boldsymbol{e_z}\times\boldsymbol{u}, \tag{2.1}$$

$$\frac{\partial \boldsymbol{C}}{\partial t} = -\boldsymbol{u}\cdot\nabla\boldsymbol{C} + \boldsymbol{C}\cdot\nabla\boldsymbol{u} + (\nabla\boldsymbol{u})^{\mathrm{T}}\cdot\boldsymbol{C} - \boldsymbol{\tau}^p. \tag{2.2}$$

The polymer stress tensor $\boldsymbol{\tau}^p$ is obtained via the Peterlin function $f(\boldsymbol{C})$ as follows:

$$\boldsymbol{\tau}^p = \frac{1}{Wi}(f(\boldsymbol{C})\boldsymbol{C} - \boldsymbol{I}), \quad f(\boldsymbol{C}) = \frac{L^2-3}{L^2\text{-trace}(\boldsymbol{C})}, \tag{2.3}$$

where $\beta = \eta_s/\eta_t$, with η_s and η_p being respectively the solvent and polymeric contributions to the total viscosity η_t, and L denotes the maximum polymer chain extension. The Weissenberg, Reynolds and rotation numbers are defined as $Wi = \lambda U_w/h$, $Re = \rho U_w h/\eta_t$ and $Ro = 2\Omega_z h/U_w$, respectively, where λ is the polymer relaxation time. It should be noted that the FENE-P model is the constitutive equation of choice for describing the ensemble-averaged chain dynamics of dilute polymeric solutions composed of linear macromolecules. In the bulk flow, a small diffusive term $\kappa\nabla^2\boldsymbol{C}$ corresponding to a Schmidt number $Sc = 1/(\kappa Re) = 0.15$ is added to (2.2) to stabilize numerical integration of the constitutive equation following Sureshkumar *et al.* (1997). As demonstrated in our prior studies (Zhu *et al.* 2020, 2022), this κ value does not modify the essential features of viscoelastic RPCF. The above equations are supplemented by no-slip boundary conditions at the walls, as well as periodic boundary conditions in the homogeneous streamwise and spanwise directions (Teng *et al.* 2018). It should also be

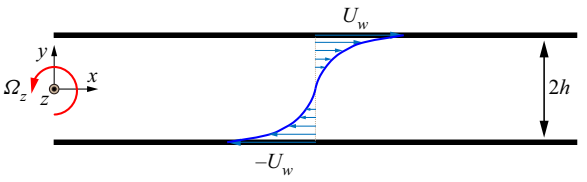

Figure 1. Sketch of spanwise-rotating plane Couette flow.

noted that the diffusive term is not added to the evolution equation for the conformation tensor at solid boundaries; thus no boundary conditions are imposed at the walls for $\boldsymbol{C}$.

A comprehensive examination of polymer-induced asymptotic states in viscoelastic RPCF at $Re = 1300$ is carried out over a broad range of $0 \leq Wi \leq 100$ and at large spanwise rotation, namely $0.3 \leq Ro \leq 0.7$ (Bech & Andersson 1996; Gai *et al.* 2016; Zhu *et al.* 2022), where the wall region is populated by Coriolis-force-generated small-scale vortices. Large values of $\beta = 0.9$ and $L = 120$ are used to ensure that the dilute polymeric solution has a nearly shear-independent viscosity and a large elongational viscosity known to play a significant role in elastically induced flow transitions in curvilinear flows. To experimentally realize the reported simulation results, two classes of polymeric solutions, namely water-soluble polymers and 'Boger' fluids, should be considered. For example, water-soluble polymers such as polyethylene oxide (PEO) and polyacrylamide (PAAM) offer the desired variability in molecular weight, namely 50 000–6 000 000 Da for PEO and 10 000–70 000 000 Da for PAAM, and the variation in persistence length, i.e. 3.7 Å and lower, to fine-tune L, λ and β as desired. Evidently, a careful mapping of molecular parameters and the specific polymer concentration is required to match the simulation and experimental parameters (Serafini *et al.* 2022). However, it is well known that the extensional rheology of polymeric solutions commonly used in this class of flows cannot be characterized via a single, L parameter. For that matter, capturing the linear viscoelastic response of the fluid requires a multi-mode description. Considering that direct numerical simulation with multi-modes and different L associated with each mode is beyond the current capabilities of the most powerful supercomputers, the computational rheology community has made the pragmatic choice of using a set of variables that closely approximate the fluid rheology of solutions used in turbulent flows of polymeric solutions. A computational domain of $L_x \times L_y \times L_z = 10\pi \times 2 \times 4\pi$ and a corresponding grid size of $N_x \times N_y \times N_z = 256 \times 129 \times 256$ with grid resolutions in wall units $\Delta x^+ \times (\Delta y^+_{min}, \Delta y^+_{max}) \times \Delta z^+ \lesssim 17.8 \times (0.04, 3.6) \times 7.1$ are used for the streamwise (x), wall-normal (y) and spanwise (z) directions, respectively (Bech & Andersson 1996; Gai *et al.* 2016; Zhu *et al.* 2020). The superscript '+' denotes hereafter a quantity non-dimensionalized by the viscous length scale. Informed by our prior studies (Zhu *et al.* 2020, 2022), calculations of $\sim 1000h/U_w$ with a small time step, i.e. $\Delta t = 0.01$ (corresponding to $\Delta t^+ \lesssim 0.088$), and a Courant–Friedrichs–Lewy number ≈ 0.11 are performed to ensure that statistically stationary flows have been realized.

3. Results and discussion

The existence of the polymer-induced MDE asymptote is clearly depicted by the Wi dependence of the frictional Reynolds number (Re_τ; see figure 2*a*) and the corresponding mean velocity profiles (see figure 2*b*). For all Ro considered, namely $Ro = 0.3$, 0.4 and 0.7, an increase in Wi from 0 to 20 results in an expected increase of Re_τ and a

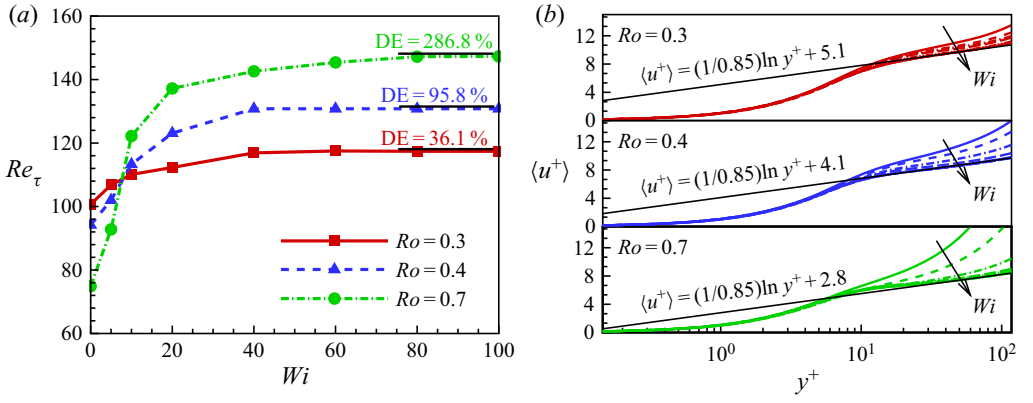

Figure 2. (*a*) Frictional Reynolds number $Re_\tau = \rho u_\tau h/\eta_t$ versus Wi at various Ro with $u_\tau = \sqrt{\tau_w/\rho}$ being the frictional velocity and τ_w the total wall stress (the sum of viscous stress and polymer stress). Here, DE is evaluated as $(Re_\tau^2 - Re_{\tau 0}^2)/Re_{\tau 0}^2$, where $Re_{\tau 0}$ is the frictional Reynolds number of the Newtonian flow. (*b*) Log plot of mean velocity profile $\langle u^+ \rangle$ in the lower half of the channel for each Ro versus wall-normal distance y^+ at $Wi = 0, 5, 10, 20, 40, 60, 80, 100$, where $\langle\ \rangle$ denotes the ensemble average. Here, $\langle u^+ \rangle \equiv \langle (u + U_w)^+ \rangle$, and hereafter $\langle u^+ \rangle = \kappa_K^{-1} \ln y^+ + B$ with $\kappa_K = 0.85$ is plotted as a visual guide. The square of the correlation coefficients R^2 between the simulation results and the linear fitting curves for $Ro = 0.3, 0.4, 0.7$ at $Wi = 100$ are obtained, respectively, as $R^2 \approx 0.993, 0.995, 0.991$.

commensurate increase of DE. However, the DE of viscoelastic RPCF eventually plateaus at $40 \leq Wi \leq 100$ (see figure 2*a*). Despite the opposite DM, the asymptotic behaviour of drag is quite similar to MDR in channel (Samanta *et al.* 2013; Sid *et al.* 2018; Shekar *et al.* 2019) and pipe (Choueiri *et al.* 2018; Lopez *et al.* 2019) flows. It should also be noted that the influence of the added global artificial diffusion on this asymptotic behaviour has been extensively examined (see the Appendix for details). Our extensive analysis shows that as Sc is increased, simulations converge to the same MDE asymptote. Hence, the MDE asymptote is an inherent dynamical property of viscoelastic RPCF in the EIT flow regime.

The velocity profile of this novel asymptotic flow state saturates to a remarkable logarithmic-like law when plotted using traditional inner variable scaling (see figure 2*b*), much like the well-known von Kármán law for NT ($\langle u^+ \rangle \approx 0.41^{-1} \ln y^+ + 5.1$) and the Virk law at MDR ($\langle u^+ \rangle \approx 11.7 \ln y^+ - 17$) (Shaqfeh & Khomami 2021). For all Ro examined, the mean velocity $\langle u^+ \rangle$ gradually decreases in the core region as Wi is increased from 0 to 20. The $\langle u^+ \rangle$ profile at $40 \leq Wi \leq 100$ appears to collapse onto a nearly identical logarithmic-like law dubbed the MDE asymptote. As a visual guide, we have plotted $\langle u^+ \rangle = \kappa_K^{-1} \ln y^+ + B$ in the region $y \gtrsim 20$. Using this fitting procedure, the MDE asymptotes at different Ro have almost the same logarithmic slope ($\kappa_K = 0.85$) but different intercepts, i.e. $B = 5.1, 4.1, 2.8$ for $Ro = 0.3, 0.4, 0.7$, respectively (see figure 2*b*). Moreover, the existence of the MDE asymptote along with its nearly identical logarithmic slope are also observed at higher Re, for example at $Re = 2600, 3900$ at $Ro = 0.7$ (see the Appendix for details). Hence, there is clear evidence of existence of MDE at high Re. To that end, to prove the universality of this finding along with the existence of a log law similar to the von Kármán law, simulations at higher Re are of paramount importance.

It should also be noted that when one examines the indicator function $\zeta = y^+ \, \mathrm{d}\langle u^+ \rangle / \mathrm{d}y^+$ (see figure 3), the $\langle u^+ \rangle$ profiles at the MDE asymptote are not a well-defined logarithmic function over a large range of y^+. In fact, the slope deviates from

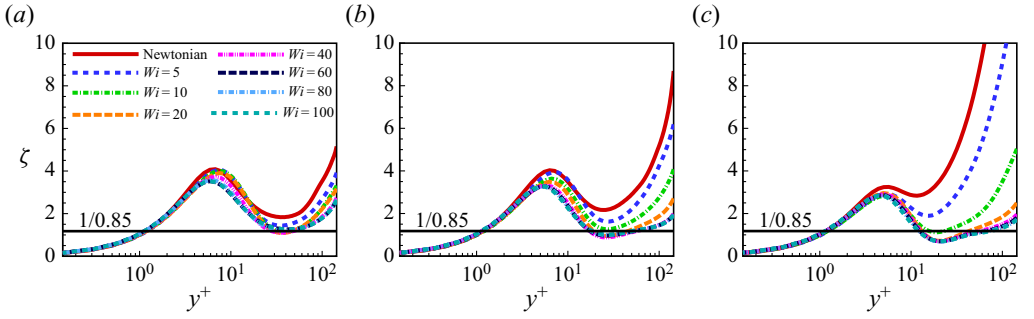

Figure 3. Indicator function $\zeta = y^+\langle u^+\rangle/\mathrm{d}y^+$ typically used to indicate logarithmic dependence of the mean velocity profile: (*a*) $Ro = 0.3$; (*b*) $Ro = 0.4$; (*c*) $Ro = 0.7$.

$\kappa_K = 0.85$ especially for $Ro = 0.7$. Such deviations of the $\langle u^+\rangle$ profiles from the logarithmic functional relationship have been reported widely for low-*Re* turbulent flows with polymer addition at the MDR asymptote (White *et al.* 2012; Elbing *et al.* 2013) and Newtonian Taylor–Couette flows (Ostilla, Verzicco & Lohse 2015, 2016). Nevertheless, the logarithmic-like profiles of a nearly identical slope clearly underscore the fact that the asymptotic states, namely MDR and MDE, are inherent properties of turbulent flow of dilute polymeric solutions. To that end, irrespective of the observed DM, the asymptotic states originate from the intricate balance between inertial and elastic forces, in the elastically dominated EIT flow state. This further underscores the universality of polymer interactions with vortical structures (Teng *et al.* 2018; Zhu *et al.* 2020, 2022).

A prototypical visualization of the flow via instantaneous snapshots of turbulent vortices at the MDE asymptote is shown in figure 4. Evidently, introducing polymer additives to NT results in an obvious suppression of turbulent vortices as also seen in DR pipe (Choueiri *et al.* 2018; Lopez *et al.* 2019) and channel (Samanta *et al.* 2013; Sid *et al.* 2018; Shekar *et al.* 2019) flows. However, as the asymptotic MDE state is approached, i.e. $40 \leq Wi \leq 100$, the dominant flow feature is that of small-scale streamwise-elongated vortices that are attached to the walls. These flow features are nearly identical to the EIT observed in viscoelastic RPCF (Zhu *et al.* 2022) where it has been unequivocally demonstrated that streamwise-elongated vortices are generated by Coriolis forces that arise due to system rotation. These findings underscore the mechanistic difference between the present rotation-driven EIT flow state and other unidirectional planar and axisymmetric shear-driven EIT. However, the combined effects of rotation and curvature in viscoelastic Taylor–Couette flow give rise to small-scale elastic Görtler vortices which are also streamwise-elongated, i.e. oriented along the azimuthal direction (Song *et al.* 2019, 2021*a*,*b*). Overall, in RPCF these rotation-rendered, namely Coriolis-force-generated, turbulent vortices give rise to significant incoherent transport and homogenization of polymer stretch/stress. To that end, it is not surprising that the EIT flow state observed in RPCF has opposite DM and flow features different from those of EIT in channel (Samanta *et al.* 2013; Sid *et al.* 2018; Shekar *et al.* 2019) and pipe (Choueiri *et al.* 2018; Lopez *et al.* 2019) flows, namely three-dimensional streamwise-oriented structures as opposed to two-dmensional spanwise-oriented structures. Note that in figure 4, the occurrence of MDE is indicated to be accompanied by an intriguing saturation of these streamwise-elongated vortices.

The saturation of small-scale vortices, i.e. in terms of number density and overall shape, is quantified by the streamwise vorticity fluctuation $\omega'^+_{x,rms}$ depicted in figure 5. It is clearly

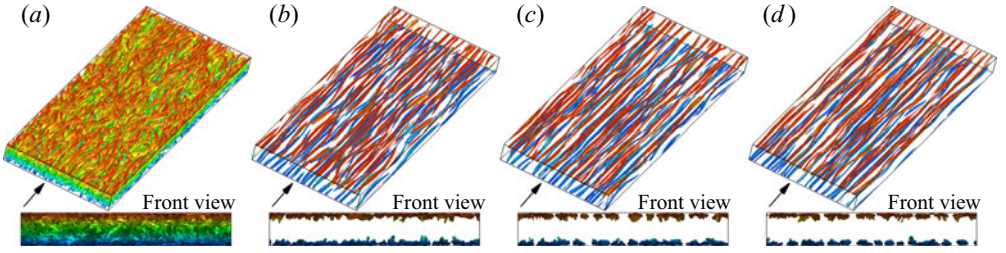

Figure 4. Instantaneous vortical structures of $Re = 1300$, $Ro = 0.7$ identified by the Q criterion with $Q = 0.2$ and coloured as a function of distance from the lower wall. The upper and lower plots are the full and front (x-direction) views, respectively. (*a*) Newtonian; (*b*) $Wi = 40$; (*c*) $Wi = 60$; (*d*) $Wi = 100$.

seen that as the MDE asymptote is approached via increasing Wi for various Ro, $\omega'^{+}_{x,rms}$ reaches an asymptotic limit across the gap. The change in $\omega'^{+}_{x,rms}$ is mainly attributed to the near-wall turbulent vortical structures (Kim *et al.* 2007). Hence, the 'saturation' of streamwise-elongated vortices at the MDE asymptote corresponds to a limiting state of small-scale vortical flows. In the EIT of viscoelastic RPCF, turbulent vortices are known to facilitate transverse momentum exchange and turbulent mixing of polymer stress via their circulations, i.e. they account for the generation of Reynolds (J^u_R) and polymer (J^u_p) stresses and thus the total drag force (Zhu *et al.* 2020, 2022). As evidenced in figure 6, J^u_R and J^u_p reach a plateau when the MDE is realized. Therefore, the asymptotic MDE state originates from saturation of turbulent vortices at $Wi \geq 40$.

The magnitudes of Reynolds and polymer stresses and their variations as a function of Wi closely capture the intrinsic competition between inertial and elastic forces that drive flow transitions from NT to EIT flows and commensurate DM (see figure 6). Evidently for the range of Ro considered, as Wi is continuously increased the magnitude of polymer stress monotonically grows and eventually becomes significantly larger than that of Reynolds stress as the MDE asymptote is approached. This underscores the fact that elastic forces play a central role in sustaining turbulence dynamics at MDE. Furthermore, an example of energy exchange between turbulent motions and polymer chains, i.e. $-P^t_p$ at $Ro = 0.7$, is shown in figure 7. In the buffer layer ($y^+ \approx 10$), $-P^t_p > 0$ indicates that stretched polymer chains release their stored elastic energy to enhance turbulent kinetic energy (TKE). For all Ro considered, the contribution of $-P^t_p$ to production of TKE is enhanced as Wi increases and eventually plateaus at the MDE state. It is noteworthy that turbulent motions in NT only extract TKE from the mean shear flow. Therefore, $-P^t_p$ works as a source term to produce TKE via releasing stored polymeric elastic energy. Hence, there are distinct differences between the mechanism by which NT and EIT flows are sustained. This in turn provides additional evidence that the asymptotic DM behaviour in viscoelastic turbulent flow of dilute polymeric solutions, namely MDR and MDE, arises due to the unique elastic nature of EIT flow state.

Taken together, the above observations clearly indicate that for all Ro considered, introducing polymer additives results in suppression of vortical structures and continuous decrease of Reynolds stress as Wi is enhanced. Hence, the asymptotic flow state is realized when elastic forces become sufficiently large and the Reynolds stress becomes vanishingly small. Clearly their ratio reaches a constant value when the MDE asymptote is reached (see figure 6). The main coherent structure at MDE is that of nearly uniform flow vortical structures (see figure 4). The aforementioned vortical structure changes as a function of Wi and the commensurate decrease in Reynolds stress are very similar to

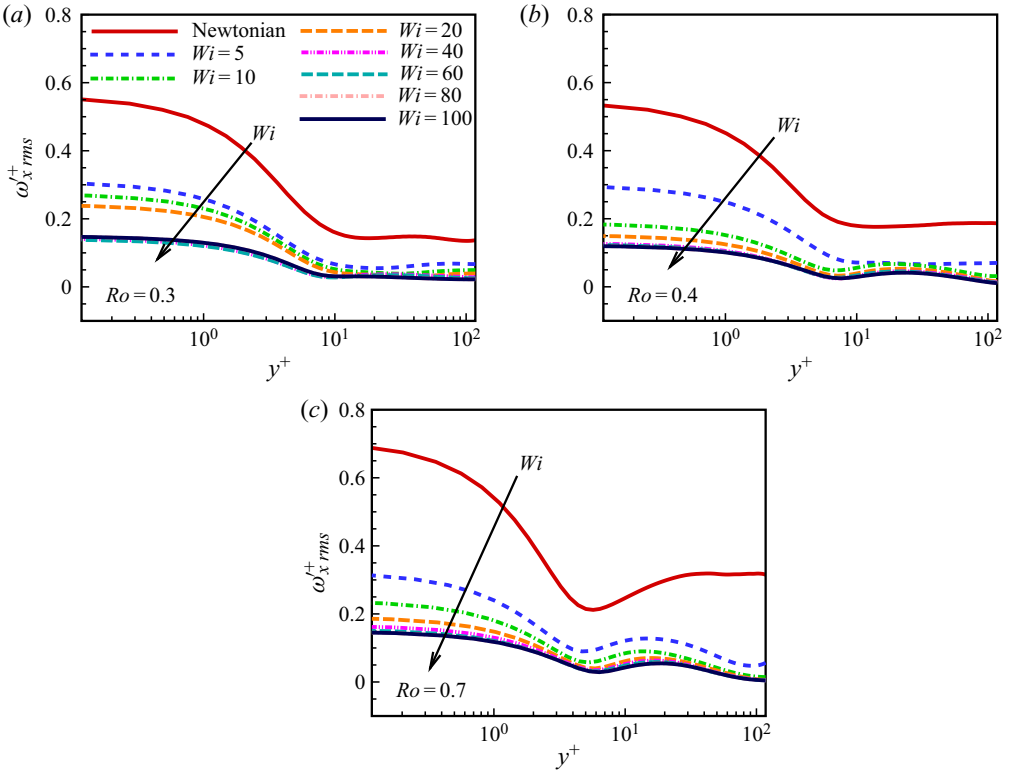

Figure 5. The root-mean-square value of streamwise vorticity fluctuation for $Wi = 0, 5, 10, 20, 40, 60, 80, 100$ at (*a*) $Ro = 0.3$, (*b*) $Ro = 0.4$ and (*c*) $Ro = 0.7$.

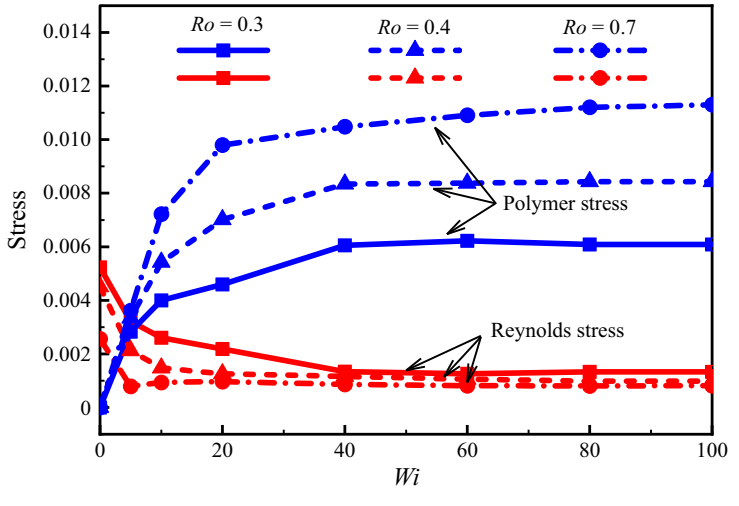

Figure 6. The volume-averaged Reynolds stress (red lines) and polymer stress (blue lines) for $Ro = 0.3, 0.4, 0.7$ calculated as $J_R^u = (1/2h)\int_{-h}^{h}\langle -u'v'\rangle \,\mathrm{d}y$ and $J_p^u = (1/2h)\int_{-h}^{h}\langle((1-\beta)/Re)\tau_{xy}^p\rangle \,\mathrm{d}y$, respectively (Zhu *et al.* 2020, 2022), where $\boldsymbol{u}' = \boldsymbol{u} - \langle\boldsymbol{u}\rangle$.

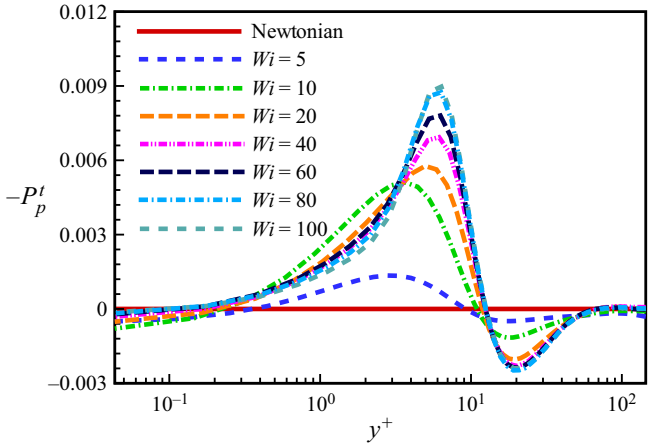

Figure 7. Energy exchange between turbulent motions and polymer chains denoted by $-P_p^t = -\langle \tau_{ik}^{p\prime}(\partial u_i'/\partial x_k)\rangle$ for $Ro = 0.7$ (Zhu *et al.* 2020, 2022).

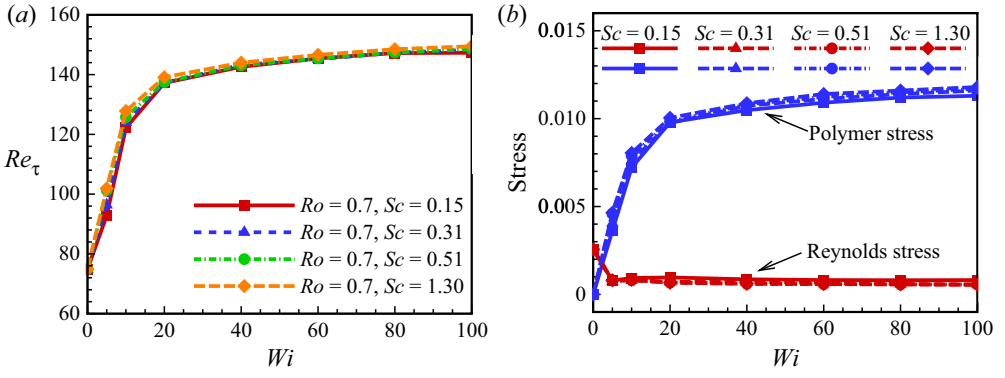

Figure 8. (*a*) Frictional Reynolds number Re_τ versus Wi at $Re = 1300$, $Ro = 0.7$, $Sc = 0.15, 0.31, 0.51, 1.30$. (*b*) Volume-averaged Reynolds stress (red lines and symbols) and polymer stress (blue lines and symbols) for $Ro = 0.7$ at various Sc.

what is seen in DR planar shear flows. Specifically, for RPCF of $Re = 1300$, $Ro = 0.4$, the Reynolds stress is reduced up to 78.1 % as Wi increases from 0 to 100; it is comparable to 85.7 % DR realized in channel flow at $Re = 6000$, $Wi = 100$ (Samanta *et al.* 2013). This points to the universality of the interplay between polymer and vortical structures at both asymptotic states, i.e. MDR and MDE. The differences in DM between turbulent viscoelastic RPCF and channel and pipe flows can be rationalized by the fact that in RPCF the Coriolis-force-generated small-scale vortices transport highly stretched polymer chains at the walls to the bulk flow. This in turn leads to incoherent transport and homogenization of polymer stress and results in notable DE (Zhu *et al.* 2022).

4. Concluding remarks

In summary, the existence of the MDE asymptote has been demonstrated for the first time via high-fidelity direct numerical simulation. Specifically, it is shown that at sufficiently large Ro, introduction of polymer additives results in DE in RPCF. The extent of DE

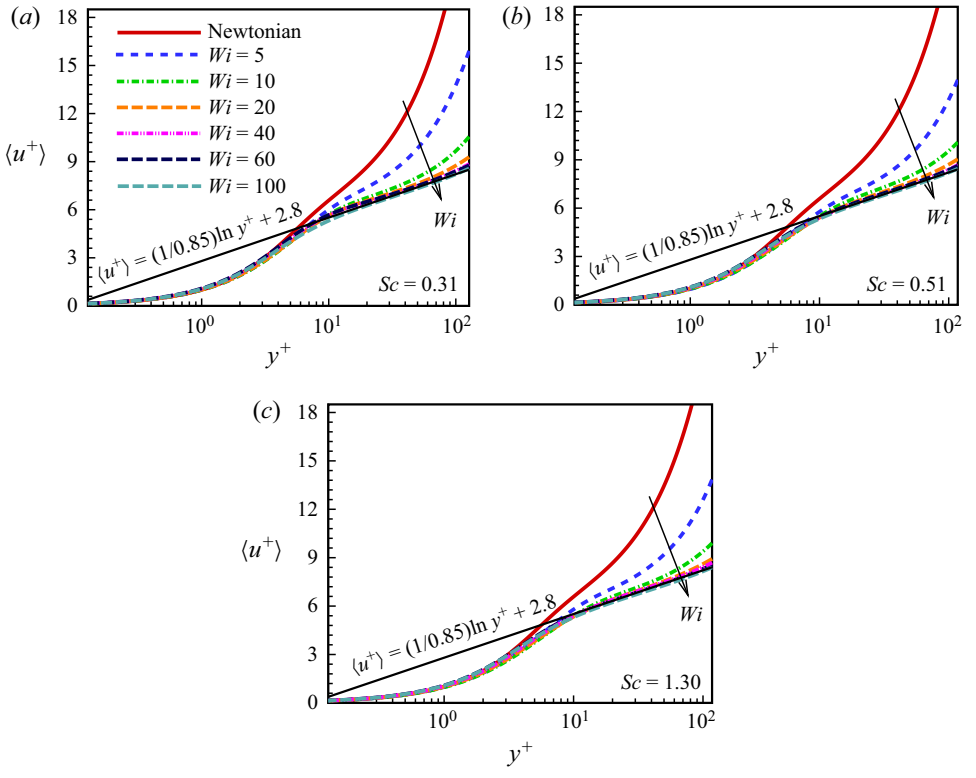

Figure 9. Log plot of mean velocity profile $\langle u^+ \rangle$ for $Re = 1300$, $Ro = 0.7$ and $Wi = 0, 5, 10, 20, 40, 60, 100$ versus wall-normal distance y^+ at (*a*) $Sc = 0.31$, (*b*) $Sc = 0.51$ and (*c*) $Sc = 1.30$. The square of the correlation coefficient R^2 of the log law of $\langle u^+ \rangle$ fitted for $Wi = 100$ is obtained as $R^2 = 0.999$, 0.998 and 0.997 for (*a–c*), respectively.

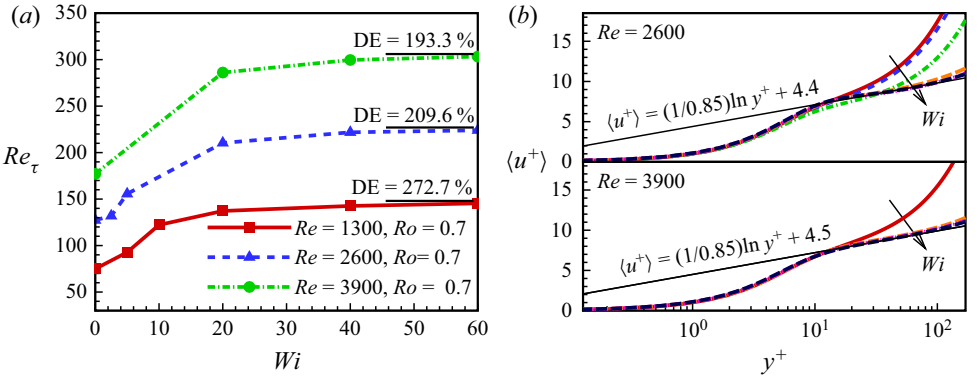

Figure 10. (*a*) Frictional Reynolds number Re_τ versus Wi at $Re = 1300$, 2600, 3900 and $Ro = 0.7$ and (*b*) the corresponding logarithmic-like mean velocity profile $\langle u^+ \rangle$ versus wall-normal distance y^+ at various Wi. For the log law of $\langle u^+ \rangle$ fitted at $Wi = 60$, R^2 is obtained as 0.991 and 0.998 for $Re = 2600$ and 3900, respectively.

gradually increases as the elastic forces are enhanced, i.e. Wi is increased, and eventually plateaus at the MDE asymptote. For the range of Ro considered, the mean velocity profiles at MDE appear to attain a remarkable logarithmic-like law characterized by a nearly identical slope, i.e. a von Kármán-like constant $\kappa_K = 0.85$. Furthermore, it has clearly been shown that the MDE asymptote is realized in the EIT flow state that is

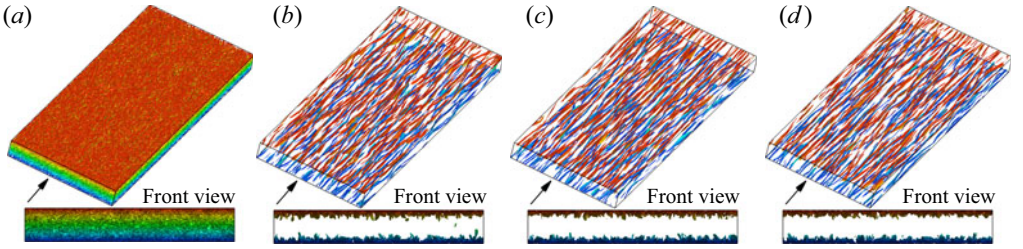

Figure 11. Prototypical instantaneous snapshots of vortical structures at $Re = 3900$, $Ro = 0.7$ identified by the Q criterion with $Q = 0.2$ and coloured as a function distance from the lower wall. The upper and lower plots are the full and front (x-direction) views, respectively. (a) Newtonian; (b) $Wi = 20$; (c) $Wi = 40$; (d) $Wi = 60$.

mainly sustained by elastic forces. Similar to pipe and channel flows, polymer additives store elastic energy in the near-wall region and in turn release this energy in the buffer layer to enhance TKE. This points to the universality of the interaction between polymer chains and vortical structures in the MDR and MDE flow states. These observations taken together demonstrate that the asymptotic behaviour seen in polymer-induced DM, i.e. MDR and MDE, is an inherent property of EIT flow state. To that end, a universal picture of elastically induced DM asymptotes is emerging, namely that these asymptotic states are an inherent property of elastically sustained EIT flow state. Hence, the discovery of the MDE asymptote has paved the way for coordinated experimental/simulation/theoretical studies in a variety of turbulent flows to establish the universality of asymptotic flow states in the EIT flow regime.

Acknowledgements. The presented calculations were performed at the Supercomputing Center of University of Science and Technology of China.

Funding. We would like to acknowledge funding from NSFC grant nos 12172353, 11621202, 92252202, 92052301, 91752110, 12172351 and NSF grant CBET0755269.

Declaration of interests. The authors report no conflict of interest.

Author ORCIDs.
Yabiao Zhu https://orcid.org/0000-0002-8591-9600;
Zhenhua Wan https://orcid.org/0000-0003-0035-3116;
Fenghui Lin https://orcid.org/0000-0002-6909-0636;
Nansheng Liu https://orcid.org/0000-0001-9128-1933;
Xiyun Lu https://orcid.org/0000-0002-0737-6460;
Bamin Khomami https://orcid.org/0000-0002-0091-2312.

Appendix

The influence of global artificial diffusion has been extensively examined via test simulations at $Re = 1300$ and $Ro = 0.7$ with a highly refined grid size of $N_x \times N_y \times N_z = 512 \times 256 \times 512$ and a much smaller time step $\Delta t = 0.0025$ (Sureshkumar & Beris 1995; Sureshkumar *et al.* 1997). The frictional Reynolds number Re_τ, the Reynolds stress and polymer stress obtained from the simulations at three different Sc show slight variation at $0 \leq Wi \leq 20$, while at $40 \leq Wi \leq 100$ they are in excellent agreement (see figure 8). Moreover, as Wi is increased from 0 to 100, the mean velocity profiles at $Sc = 0.31, 0.51, 1.30$ gradually collapse into a log-law regime similar to the simulations at $Sc = 0.15$. This indicates that in the mesh/Sc range used in this study, global artificial

diffusion does not alter the reported logarithmic slope (see figure 9). These excellent agreements at $40 \leq Wi \leq 100$ at which the MDE asymptote is observed clearly underscore the accuracy of our reported results and the fact that MDE is an inherent dynamical property of viscoelastic RPCF.

Moreover, the influence of Re on the MDE asymptote has been examined by simulations at $Re = 2600$ and 3900 at $Ro = 0.7$, $Wi = 0$–60. The highest Re is calculated with a much finer grid size of $N_x \times N_y \times N_z = 512 \times 256 \times 512$ and a smaller time step $\Delta t = 0.005$. The introduction of polymer additives results in an obvious increase of Re_τ, and a commensurately large DE. Similar to the simulation results at $Re = 1300$, the DE basically reaches a plateau at $40 \leq Wi \leq 60$ (see figure 10*a*). Moreover, the mean velocity $\langle u^+ \rangle$ at the MDE asymptote closely follows the visual guide $\langle u^+ \rangle = (1/0.85) \ln y^+ + 4.4$ for $Re = 2600$ and $\langle u^+ \rangle = (1/0.85) \ln y^+ + 4.5$ for $Re = 3900$. The fact that at the Re considered the logarithmic-like profiles have an identical slope demonstrates that the reported MDE asymptote is not a sensitive function of Re.

As noted above, the MDE asymptotic state is an EIT flow state as evidenced by the presence of small-scale streamwise-elongated vortices attached to the walls (see figure 11). This suggests that the turbulent flow state and the elastic nature of MDE could be universal for this class of flows. However, the Re values considered in the present study are still relatively low in comparison to Re at which the log law is studied in NT. Hence, simulations at higher Re are of paramount importance in establishing the universality of MDE and the existence of a von Kármán-like log law seen in high-Re turbulent Newtonian flows.

References

Bech, K.H. & Andersson, H.I. 1996 Secondary flow in weakly rotating turbulent plane Couette flow. *J. Fluid Mech.* **317**, 195–214.

Brauckmann, H.J., Salewski, M. & Eckhardt, B. 2016 Momentum transport in Taylor–Couette flow with vanishing curvature. *J. Fluid Mech.* **790**, 419–452.

Choueiri, G.H., Lopez, J.M. & Hof, B. 2018 Exceeding the asymptotic limit of polymer drag reduction. *Phys. Rev. Lett.* **120** (12), 124501.

De Angelis, E., Casciola, C.M. & Piva, R. 2002 DNS of wall turbulence: dilute polymers and self-sustaining mechanisms. *Comput. Fluids* **31**, 495–507.

Dubief, Y., Terrapon, V.E., White, C.M., Shaqfeh, E.S., Moin, P. & Lele, S.K. 2005 New answers on the interaction between polymers and vortices in turbulent flows. *Flow Turbul. Combust.* **74**, 311–329.

Elbing, B.R., Perlin, M.R., Dowling, D. & Ceccio, S.L. 2013 Modification of the mean near-wall velocity profile of a high-Reynolds number turbulent boundary layer with the injection of dragreducing polymer solutions. *Phys. Fluids* **25**, 085103.

Gai, J., Xia, Z., Cai, Q. & Chen, S. 2016 Turbulent statistics and flow structures in spanwise-rotating turbulent plane Couette flows. *Phys. Rev. Fluids* **1** (5), 054401.

Kim, K., Li, C.-F., Sureshkumar, R., Balachandar, S. & Adrian, R.J. 2007 Effects of polymer stresses on eddy structures in drag-reduced turbulent channel flow. *J. Fluid Mech.* **584**, 281–299.

Li, C.-F., Sureshkumar, R. & Khomami, B. 2006 Influence of rheological parameters on polymer induced turbulent drag reduction. *J. Non-Newtonian Fluid Mech.* **140** (1–3), 23–40.

Li, C.-F., Sureshkumar, R. & Khomami, B. 2015 Simple framework for understanding the universality of the maximum drag reduction asymptote in turbulent flow of polymer solutions. *Phys. Rev.* E **92**, 043014.

Liu, N. & Khomami, B. 2013 Polymer-induced drag enhancement in turbulent Taylor–Couette flows: direct numerical simulations and mechanistic insight. *Phys. Rev. Lett.* **111**, 114501.

Lopez, J.M., Choueiri, G.H. & Hof, B. 2019 Dynamics of viscoelastic pipe flow at low Reynolds numbers in the maximum drag reduction limit. *J. Fluid Mech.* **874**, 699–719.

Lumley, J.L. 1969 Drag reduction by additives. *Annu. Rev. Fluid Mech.* **1**, 367–384.

Ostilla, R., Verzicco, R. & Lohse, D. 2015 Effects of the computational domain size on direct numerical simulations of Taylor–Couette turbulence with stationary outer cylinder. *Phys. Fluids* **27**, 025110.

OSTILLA, R., VERZICCO, R. & LOHSE, D. 2016 Turbulent Taylor–Couette flow with stationary inner cylinder. *J. Fluid Mech.* **766**, R1.

PROCACCIA, I., L'VOV, V.S. & BENZI, R. 2008 Colloquium: theory of drag reduction by polymers in wall-bounded turbulence. *Rev. Mod. Phys.* **80**, 225–247.

SALEWSKI, M. & ECKHARDT, B. 2015 Turbulent states in plane Couette flow with rotation. *Phys. Fluids* **27** (4), 045109.

SAMANTA, D., DUBIEF, Y., HOLZNER, M., SCHÄFER, C., MOROZOV, A.N., WAGNER, C. & HOF, B. 2013 Elasto-inertial turbulence. *Proc. Natl Acad. Sci. USA* **110** (26), 10557–10562.

SERAFINI, F., BATTISTA, F., GUALTIERI, P. & CASCIOLA, C.M. 2022 Drag reduction in turbulent wall-bounded flows of realistic polymer solutions. *Phys. Rev. Lett.* **129**, 104502.

SEYER, F.A. & METZNER, A.B. 1969 Turbulence phenomena in drag-reducing systems. *AIChE J.* **15**, 426.

SHAQFEH, E.S.G. & KHOMAMI, B. 2021 The Oldroyd-B fluid in elastic instabilities, turbulence and particle suspensions. *J. Non-Newtonian Fluid Mech.* **298**, 104672.

SHEKAR, A., MCMULLEN, R.M., WANG, S.-N., MCKEON, B.J. & GRAHAM, M.D. 2019 Critical-layer structures and mechanisms in elastoinertial turbulence. *Phys. Rev. Lett.* **122** (12), 124503.

SID, S., TERRAPON, V.E. & DUBIEF, Y. 2018 Two-dimensional dynamics of elasto-inertial turbulence and its role in polymer drag reduction. *Phys. Rev. Fluids* **3** (1), 011301.

SONG, J., LIN, F., LIU, N., LU, X. & KHOMAMI, B. 2021*a* Direct numerical simulation of inertio-elastic turbulent Taylor–Couette flow. *J. Fluid Mech.* **926**, A37.

SONG, J., TENG, H., LIU, N., DING, H., LU, X. & KHOMAMI, B. 2019 The correspondence between drag enhancement and vortical structures in turbulent Taylor–Couette flows with polymer additives: a study of curvature dependence. *J. Fluid Mech.* **881**, 602–616.

SONG, J., WAN, Z., LIU, N., LU, X. & KHOMAMI, B. 2021*b* A reverse transition route from inertial to elasticity-dominated turbulence in viscoelastic Taylor–Couette flow. *J. Fluid Mech.* **927**, A10.

SURESHKUMAR, R. & BERIS, A.N. 1995 Effect of artificial stress diffusivity on the stability of numerical calculations and the flow dynamics of time-dependent viscoelastic flows. *J. Non-Newtonian Fluid Mech.* **60** (1), 53–80.

SURESHKUMAR, R., BERIS, A.N. & HANDLER, R.A. 1997 Direct numerical simulation of the turbulent channel flow of a polymer solution. *Phys. Fluids* **9** (3), 743–755.

TENG, H., LIU, N., LU, X. & KHOMAMI, B. 2018 Turbulent drag reduction in plane Couette flow with polymer additives: a direct numerical simulation study. *J. Fluid Mech.* **846**, 482–507.

TOMS, B.A. 1949 Some observations on the flow of linear polymer solutions through straight tubes at large Reynolds numbers. In *Proceedings of the International Congress on Rheology*, pp. 135–141. North Holland.

VIRK, P.S. 1975 Drag reduction fundamentals. *AIChE J.* **21** (4), 625–656.

WHITE, C.M., DUBIEF, Y. & KLEWICKI, J. 2012 Re-examining the logarithmic dependence of the mean velocity distribution in polymer drag reduced wall-bounded flow. *Phys. Fluids* **24**, 021701.

WHITE, C.M. & MUNGAL, M.G. 2008 Mechanics and prediction of turbulent drag reduction with polymer additives. *Annu. Rev. Fluid Mech.* **40**, 235–256.

ZHU, Y., SONG, J., LIN, F., LIU, N., LU, X. & KHOMAMI, B. 2022 Relaminarization of spanwise-rotating viscoelastic plane Couette flow via a transition sequence from a drag-reduced inertial to a drag-enhanced elasto-inertial turbulent flow. *J. Fluid Mech.* **931**, R7.

ZHU, Y., SONG, J., LIU, N., LU, X. & KHOMAMI, B. 2020 Polymer-induced flow relaminarization and drag enhancement in spanwise-rotating plane Couette flow. *J. Fluid Mech.* **905**, A19.